Ironmaking & Steelmaking

Processes, Products and Applications

ISSN: (Print) (Online) Journal homepage: https://www.tandfonline.com/loi/yirs20

CFD modelling of steel desulfurisation in a gas-stirred ladle

Congshan Mao, Xipeng Guo, Nicholas J. Walla, Armin K. Silaen, Vivek Thapliyal & Chenn Q. Zhou

To cite this article: Congshan Mao, Xipeng Guo, Nicholas J. Walla, Armin K. Silaen, Vivek Thapliyal & Chenn Q. Zhou (2023): CFD modelling of steel desulfurisation in a gas-stirred ladle, Ironmaking & Steelmaking, DOI: 10.1080/03019233.2023.2195308

To link to this article: https://doi.org/10.1080/03019233.2023.2195308

Published online: 20 May 2023.

IRONMAKING & STEELMAKING
https://doi.org/10.1080/03019233.2023.2195308

I·M3 Institute of Materials, Minerals & Mining

Taylor & Francis
Taylor & Francis Group

RESEARCH ARTICLE

CFD modelling of steel desulfurisation in a gas-stirred ladle

Congshan Mao[a], Xipeng Guo[a], Nicholas J. Walla[a], Armin K. Silaen[a], Vivek Thapliyal[b] and Chenn Q. Zhou[a]

[a]Center for Innovation through Visualization and Simulation, Purdue University Northwest, Hammond, IN, USA; [b]Nucor Steel, Blytheville, AR, USA

ABSTRACT

Low sulfur content is crucial in secondary steelmaking to enhance steel quality. The desulfurization rate is influenced by slag-steel interactions, including slag eye size and interfacial mass transfer coefficient. Gas-stirred ladles can impact the interaction through stirring conditions such as argon flow rate and dual plug separation angle. Using a 3D CFD simulation model, the effects of different stirring conditions on the desulfurization rates, molten steel flow, and slag-steel interfacial behaviors were investigated. Results showed that 180° separation angle leads to higher desulfurization efficiency than 90°. A higher argon gas flow rate increases desulfurization rate, and using 20 SCFM ($8.92\times10_{-3}$ Nm_3/s) argon flow rate for both plugs resulted in higher desulfurization rate than using 5 SCFM ($2.23\times10_{-3}$ Nm_3/s) for one plug and 20 SCFM for the other. The smallest desulfurization efficiency was observed when using 5 SCFM for both plugs.

ARTICLE HISTORY
Received 22 September 2022
Revised 20 March 2023
Accepted 21 March 2023

KEYWORDS
CFD; Ladle; Multiphase flow; Steel desulfurization; Mass transfer; Turbulence flow; Slag eye; Argon gas injection

Introduction

desulfurisation is one of the most significant factors in making high-quality steel. Sulfur lowers steel's strength and internal cohesion and contributes to steel brittleness and fractures, diminishing resistance and durability. Therefore, the improvement of sulfur content management and desulfurisation efficiency have become crucial goals in secondary steelmaking.

As the last stage before continuous casting, ladle refining should improve the efficiency of sulfur removal and reduce sulfur content as much as possible. In a gas-stirred ladle, the desulfurisation mainly depends on the chemical reactions between slag and steel [1], as described in the equation below:

$$[S] + (CaO) = [O] + (CaS) \quad (1)$$

where [] stands for the species from the steel and () represents the species in slag.

It is commonly acknowledged that the reaction rate is mainly affected by both the sulfur distribution ratio between steel and slag at the equilibrium state and the sulfur transport process at the interface [2–5]. The equilibrium state is influenced by the chemical compositions of slag and steel, while the sulfur transport process is controlled by the interface behaviours, including interfacial mass transfer coefficient and slag eye size. In a gas-stirred ladle, the interface behaviors are mainly influenced by stirring parameters such as argon gas flow rate and plug separation angle. Therefore, it is essential to build a numerical simulation model for predicting the effect of stirring conditions on desulfurisation efficiency.

The numerical studies of ladle desulfurisation can be briefly divided into two types: (1) numerical models of parameters involved in desulfurisation; (2) effects of different conditions on desulfurisation efficiency.

In the first type, the sulfur capacity and the sulfur distribution ratio are in focus. Based on experimental works, Fincham and Richardson [6] found that the sulfur is mainly held as sulfide in slag and the capacity to hold sulfur is affected by the activity of the basic metal oxide and the sulfur capacity is therefore affected by the slag compositions. However, the empirical model was not proposed in this study. Sommerville et al. [7] developed a mathematical model for estimating the sulfide capacity between 1400°C and 1700°C by using the optical basicity. The simulation results agree well with measured data when the sulfide capacity is not too big. However, the prediction accuracy is smaller at a higher sulfide capacity. Young et al. [8] proposed a new empirical model for predicting sulfide capacity with a larger range and found that the errors between the calculated values and measured values are less than 5%. More models are developed later to predict the sulfide capacity [9–12].

Sulfur partition ratio or sulfur distribution ratio stands for the sulfur content ratio between slag and steel at the equilibrium state. Inoue and Suito [13] measured the sulfur distribution ratio with different types of slag and summarised the slag capacity with different compositions. But the impact of temperature is not well discussed and the mathematical model is not built. Chan and Fruehan [14] developed a numerical model, showing that the sulfur distribution ratio is a function of sulfide capacity, sulfur activity, oxygen activity and temperature, and the simulation results agree well with measurement data. Andersson et al. [15] summarised various approaches for determining sulfide capacity and the sulfur distribution ratios are also obtained and discussed their reliability compared to plant trials. Jeong et al. [16] investigated the desulfurisation behaviour through experiments and found that the sulfuide capacity and sulfur distribution ratio increase with the growth of the ratio between CaO and SiO_2, which can enhance the desulfurisation efficiency.

In addition to the researches focusing on particular parameters, many numerical investigations, including static mathematical model and CFD model, have been developed to predict the desulfurisation efficiency during the ladle

CONTACT Chenn Q. Zhou czhou@pnw.edu Center for Innovation through Visualization and Simulation, Purdue University Northwest, Hammond, IN 46323, USA

refining process. Jonsson et al. [17] established a 2D CFD model for predicting sulfur and aluminum transfer rates between slag and steel in a gas-stirred ladle, assuming the slag-steel interface was a flat surface. The predicted final sulfur content is about 0.007% to 0.008%, while the industrial data is 0.005% to 0.01%. Although the difference between plant data and simulation result is not very small, it shows the potential to develop a desulfurisation prediction model through CFD. Andersson et al. [18] developed a 2D CFD model for predicting both desulfurisation and reoxidation in a ladle. The activities of oxides in slag were investigated, and the impacts of compositions in slag and steel on reaction rate were discussed. The results show that the contents of alloying elements, including Al, Si and Mn, are well estimated with errors less than 5% compared to plant data. However, the desulfurisation rate is under estimated and error of S content is 25% compared to plant data. Later Andersson et al. [19] presented a 3D mathematical model as well as a static model. Both models show good behaviours in predicting desulfurisation processes. It is found that the slag composition (the ratio Al_2O_3/CaO) could have a substantial effect on the sulfur distribution.

Conejo et al. [5] updated the static mathematical model by introducing the mass balance for oxygen used by desulfurisation and reoxidation at the slag-steel interface and predicted the composition profile of both slag and steel during the ladle refining process. It is found that when the argon flow rate is less than 10 m^3/h, the desulfurisation rate is very low; when the argon flow rate is higher than 50 m^3/h, the desulfurisation efficiency almost remains unchanged even with a higher argon flow rate. Lou and Zhu [2] proposed a 3D CFD model which estimates both the desulfurisation and reoxidation coupled with fluid dynamics in a gas-stirred ladle. In this model, the slag-steel interface is a flat surface, and the slag phase is not built in the computational domain, while the change of compositions in the slag is introduced by user-defined functions. The results show that larger slag basicity can result in a higher desulfurisation rate. However, the effects of distorts and emulsification on desulfurisation efficiency are not considered with a flat surface. Singh et al. [20] built an uncoupled CFD-thermodynamic model with a curve surface to predict the desulfurisation rate in a gas-stirred ladle instead of a simple flat interface and the influence of curve interface on the interfacial area and mass transfer coefficient were discussed. It is found that the interfacial area is bigger, and the growing trend of mass transfer coefficient is also higher when using a curve surface rather than a flat surface, which is similar to some experimental reports. Although it is noticed that the predicted sulfur content of the uncoupled model is slightly higher than that of a coupled model, this uncoupled model still predicts the sulfur removal rate well compared to plant data with much less time and computing resources than the coupled model. To improve the simulation accuracy, Cao [21] developed a coupled 3D CFD model calculating the multiphase flow field, slag-steel interface behaviours and desulfurisation rate simultaneously in each step, describing the multiphase flow and species transport process accurately in a ladle. However, it requires lots of time and computational resources, which may not be practical as a tool to guide the industrial process. Later, Cao [21] and Cao et al. [22] established a static mathematical model for quickly evaluating the desulfurisation kinetics in a gas-stirred ladle. Although it shows that the simulation accuracy is not as good as in the 3D CFD model, it takes less time and computational resources, which can be applied to predict the sulfur content with a quick response roughly. Besides the studies of the desulfurisation rates with different stirring conditions and slag/steel compositions, Oliveira Pezzin et al. [23] investigated the impact of liquid and solid phase on desulfurisation rate through numerical simulation, and it is found that the percentage of liquid phase or solid phase in slag can affect the desulfurisation rate, and there is an optimal ratio of liquid–solid percentage to obtain the maximum desulfurisation efficiency. To improve the desulfurisation efficiency, the desulfurisation agent powder, such as CaO and Mg, are injected into the ladle to promote the sulfur removal rate. Moosavi-Khoonsari et al. [24] developed a 3D CFD model for predicting the desulfurisation rate by taking both interfacial reaction and injected powder reaction, which is validated by plant data. However, the effect of slag eye is not discussed in this paper. To promote the desulfurisation rate by injected power, the impeller is used to improve the mixing efficiency. Jia et al. [25] proposed a 3D CFD model and investigated the desulfurisation efficiency with different carrier gas flow rates and lance positions. It is found that a higher carrier gas flow results in a bigger desulfurisation rate, while the influence of lance positions is negligible. But the effect of slag phase on desulfurisation is not considered.

The assumption of a flat slag-steel interface can be applied to a CFD model for predicting the desulfurisation rate [2]. However, the interactions between slag and steel are not considered, and the deformation of the slag-steel interface during the ladle refining is ignored, which does not reflect the actual physical situation. Meanwhile, it will cost a lot of computing time and power to simulate the transient slag-steel interface interactions and behaviours [21]. The interfacial area slightly fluctuates around specific values when the boundary conditions remain the same during refining [21]. Therefore, the quasi-steady state is considered to simulate the interface behaviours: the multiphase flow fields are regarded to keep unchanged when parameters such as velocity remain almost stable, which can calculate the interactions between slag and steel with less time and resource consumption.

The goal of this paper is to develop a three-dimensional CFD model for predicting the slag-steel interface behaviours and desulfurisation efficiency in a gas-stirred ladle within certain scenarios in an industrial ladle and propose some suggestions to improve the desulfurisation efficiency in the industrial ladles.

Computational model

Model assumption

The following assumptions are made to build the desulfurisation model in a gas-stirred ladle:

1. The temperature gradients within slag and steel phases are ignored;
2. The argon bubble is assumed to be spherical, and it can only escapes from the top of the ladle;
3. The argon bubble diameter varies due to bubble collision, coalescence and breakup;

4. The chemical reaction rates are controlled by species mass transport process, and the transport rate is affected by the mass transfer coefficient at the slag-steel interface;
5. The species mass fraction in slag is assumed to be homogeneous because of the small size compared to steel height;
6. The species in steel phase are uniformly distributed at the beginning of the treatment;
7. The influence of the change in slag and steel composition on flow field is ignored.

Multiphase flow

The Volume of Fluid (VOF) model is used in this model to simulate the interactions between slag and steel, which are considered to be continuous phases. The argon gas is treated as a discrete phase, and the Discrete Phase Model (DPM) model is applied to calculate the bubble trajectory and the interactions between continuous and discrete phases in a gas-stirred ladle. In the steel phase, the Species Transport model is employed to calculate the sulfur transport and distribution.

VOF model

The mass conservation is described by the continuity equation as expressed by the following equation:

$$\frac{\partial \rho}{\partial t} + \nabla \cdot (\rho \vec{v}) = 0 \tag{2}$$

For the momentum conservation, the following equation is solved in VOF model:

$$\frac{\partial}{\partial t}(\rho \vec{v}) + \nabla \cdot \rho \vec{v}\vec{v} = -\nabla p + \nabla \cdot [\mu(\nabla \vec{v} + \vec{v}^T)] + \rho \vec{g} + \vec{F}_b \tag{3}$$

where $\vec{v}$ is the velocity of the continuous flows; p is the local pressure; μ is the effective viscosity of continuous phases; $\vec{g}$ is the local gravity acceleration; F_b is the bubble force exerted by the discrete phase on the mixture continuous fluids, which is the reaction force of the sum of drag force, buoyancy force, virtual mass force and the pressure gradient force acting on the discrete phase, and more details can be found in the Discrete Phase Model.

By tracking the volume fraction α of each phase in the domain, the VOF approach calculates the surfaces between phases and determines the interface sites. For the phase m_{th}, the volume fraction equation is expressed as follows:

$$\frac{\partial \alpha_m}{\partial t} + \vec{v} \cdot \nabla \alpha_m = 0 \tag{4}$$

and the sum of volume fraction of each phase equals to 1 as described below:

$$\sum \alpha_m = 1 \tag{5}$$

Discrete phase model

In this study, argon bubble is treated as a discrete phase. The Discrete Phase Model (DPM) based on the Euler–Lagrange approach is applied to determine the trajectory of each bubble by solving the force balance equation shown below, which includes drag force, buoyancy force, virtual mass force, and pressure gradient force [3]:

$$\frac{d\vec{v}_p}{dt} = F_D(\vec{v} - \vec{v}_p) + \frac{\vec{g}(\rho_p - \rho)}{\rho_p} + \vec{F}_{VM} + \vec{F}_{pressure} \tag{6}$$

where $F_D(\vec{v} - \vec{v}_p)$ is the drag force per unit particle mass. $\vec{v}$ is the continuous phase velocity and $\vec{v}_p$ is the bubble particle velocity. F_D is written as:

$$F_D = \frac{18\mu C_D R_e}{24\rho_p d_p^2} \tag{7}$$

where R_e is the particle Reynolds number based on the particle diameter and relative fluid velocity and can be written in the following format:

$$R_e = \frac{\rho d_p |v - v_p|}{\mu_l} \tag{8}$$

C_D is the drag coefficient and can be defined as:

$$C_D = \frac{2}{3}(\frac{E_0}{3})^{0.5} \tag{9}$$

where E_0 is the Eotvos number describing the relationship between buoyancy force and particle surface tension and can be calculated by the following equation:

$$E_0 = \frac{g(\rho - \rho_p)d_p^2}{3}\sigma \tag{10}$$

where σ is the surface tension between continuous phase and discrete phase. The virtual mass force $\vec{F}_{VM}$ stands for the acceleration of fluids surrounding the particle and is defined as:

$$\vec{F}_{VM} = \frac{1}{2}\frac{\rho}{\rho_p}\left(\vec{v}_p \nabla \vec{v} - \frac{d\vec{u}_p}{dt}\right) \tag{11}$$

An additional force caused by the pressure gradient will be exerted to the continuous fluids when the mixture density of continuous phases is higher than the discrete phase, which can be calculated by the following equation:

$$F_{pressure} = \left(\frac{\rho}{\rho_p}\right)\vec{v}_p \nabla \vec{v} \tag{12}$$

where $\vec{v}$ is the fluid velocity; $\vec{v}_p$ is the particle velocity; ρ and ρ_p are the density of continuous phase and discrete phase, respectively. To simulate the turbulent dispersion effect of the argon gas on the continuous phases, the bubble movement is characterised by the random walk model and two-way turbulence coupling model. The initial bubble diameter d_b^0 can be calculated by the following equation [3,26]:

$$d_b^0 = 0.091\left(\frac{\sigma}{\rho}\right)^{0.5} u_b^{0.44} \tag{13}$$

where σ is the surface tension of steel; ρ is the density of steel; u_b is the argon velocity at the inlet, which can be solved by the following equation [26]:

$$u_b = \frac{P_0 T_1}{(P_0 + (\rho_m H + \rho_s h)g)T_0}\frac{Q_0}{A} \tag{14}$$

where P_0 and T_0 are the pressure and temperature at the standard condition; T_1 is the local temperature; ρ_m is the density of steel and ρ_s is the density of slag; H is the height of molten steel and h is the thickness of the slag; A is the inlet area; Q_0 is the argon gas flow rate. The impacts of bubble collision,

coalescence, and breakup on the discrete phase are taken into consideration. It is assumed that two bubbles collide with each other and coalesce into a bigger bubble, and it breaks apart into smaller particles when its diameter is larger than the equilibrium diameter [3,26]. The collision and coalescence model is described by the algorithm of Cao and Nastac [3]. Coalescence occurs if two bubbles collide directly; a bounce occurs if they collide more obliquely. In the breakup model, the equilibrium diameter is 40 mm and two small bubbles of the same size are formed as long as the size is bigger than the equilibrium diameter [3]. Based on mass conservation, the mass of two small bubbles equals the previous one big bubble. The local pressure and temperature determine the density of the gas, and therefore the diameter of small new bubbles formed after the breakup can be obtained. This calculation is introduced by UDF code to the DPM model.

Turbulence model

The realisable $k-\varepsilon$ model is utilised to account for multiphase turbulent flow in this study. The following are the conservation equations for turbulence kinetic energy and turbulence dissipation rate [3,26]:

$$\frac{\partial}{\partial t}(\rho k)+\nabla\cdot(\rho k\vec{u})=\nabla\cdot\left[\left(\mu+\frac{\mu_t}{\sigma_k}\right)\nabla k\right]+G_k+G_b-\rho\varepsilon \tag{15}$$

$$\frac{\partial}{\partial t}(\rho\varepsilon)+\nabla\cdot(\rho\varepsilon\vec{u})=\nabla\cdot\left[\left(\mu+\frac{\mu_t}{\sigma_\varepsilon}\right)\nabla\varepsilon\right]-\rho C_1 S_\varepsilon-\rho C_2\frac{\varepsilon^2}{k+\sqrt{\nu\varepsilon}}+C_{1\varepsilon}\frac{\varepsilon}{k}C_{3\varepsilon}C_b \tag{16}$$

$$C_1=max\left[\frac{\Phi}{5+\Phi},0.43\right] \tag{17}$$

$$\Phi=S\frac{k}{\varepsilon} \tag{18}$$

$$S=\sqrt{2S_{ij}S_{ij}} \tag{19}$$

$$S_{ij}=\frac{1}{2}\left(\frac{\partial u_j}{\partial x_i}+\frac{\partial u_i}{\partial x_j}\right) \tag{20}$$

where G_k and G_b are the turbulence kinetic energy that come from velocity gradient and buoyancy, respectively. $C_{1\varepsilon}$ and C_2 are constants in this model. S_k and S_ε are the source terms of turbulence kinetic energy and turbulence dissipation rate, respectively. S is the mean rate of strain tensor that can leads to the C_1.

$$G_k=-\rho\overline{u_t'u_l'}\frac{\partial u_j}{\partial x_i} \tag{21}$$

$$G_b=\beta g_i\frac{\mu_t}{Pr_t}\frac{\partial T}{\partial x_i} \tag{22}$$

μ_t stands for the eddy viscosity and can be calculated by the following equation:

$$\mu_t=\rho C_\mu\frac{k^2}{\varepsilon} \tag{23}$$

where C_μ in realisable $k-\varepsilon$ model is obtained from:

$$C_\mu=\frac{1}{A_0+A_S\frac{kU}{\varepsilon}} \tag{24}$$

where A_0 is 4.04 in this study, and $A_S=\sqrt{6}\cos\Phi$.

$$U=\sqrt{S_{ij}S_{ij}+\tilde{\Omega}_{ij}\tilde{\Omega}_{ij}} \tag{25}$$

In Eq. (16), the term $C_{3\varepsilon}$ accounts for the proportion of the buoyancy's impacts on ε, and can be computed by the following equation:

$$C_{3\varepsilon}=\tanh\left|\frac{v}{\nu}\right| \tag{26}$$

where ν is the flow viscosity and v is the flow velocity along the gravitational vector. The other constants in Eq. (16) are $C_{1\varepsilon}=1.44$, $C_2=1.9$, $\sigma_k=1.0$, and $\sigma_\varepsilon=1.2$, as described in Cao's work [3].

Species transport model

The species transport model is used in this study to predict the local mass fraction of the species in steel phase and slag phase and the transfer rate in the same phase or between continuous phases written in the following form:

$$\frac{\partial}{\partial t}(\rho Y_i)+\nabla(\rho\vec{v}Y_i)=\nabla\cdot\left(\left(\frac{\mu_t}{Sc_t}+\rho D_{i,m}\right)(\nabla Y_i)\right)+S_i \tag{27}$$

where ρ, $\vec{v}$ and μ_t are the fluid mixture density, velocity of continuous phases and kinematic viscosity, respectively; Y_i is the local mass fraction of species in the continuous liquids; $D_{i,m}$ is the mass diffusion coefficient for species i in the mixture; S_i is the source term of species i due to the species exchange at the slag-steel interface; Sc_t is the turbulent Schmidt number and it is 0.7 by default.

Desulfurisation model

As mentioned above, the dissolved sulfur in steel reacts with lime in slag at the interface described in Eq. (1). The source term of sulfur at the interface due to desulfurisation reaction can be expressed as the following equation in terms of two-film theory [2,4,5,21]:

$$S_S=\frac{\rho_m A}{100V}k_{eff,S}\left\{[\%-S]-\frac{(\%-S)}{L_S}\right\} \tag{28}$$

where A is the local area of slag-steel interface, which is the area of the normal face of each cell at the interface; V is the cell volume of steel phase at the interfacial zone; $[\%-S]$ and $(\%-S)$ represent the local mass fraction of sulfur in steel and slag; L_S is the sulfur distribution ratio; $k_{eff,S}$ is the overall sulfur transfer coefficient of sulfur between slag and steel and can be obtained by the following equation

$$k_{eff,S}=\frac{\rho_s k_{s,S}}{\frac{\rho_m}{L_S}+\frac{\rho_s k_{s,S}}{k_{m,S}}} \tag{29}$$

where $k_{m,S}$ and $k_{s,S}$ stand for the sulfur transfer coefficient in steel phase and slag phase; ρ_m is the density of steel and ρ_s is the density of slag. Therefore, the desulfurisation rate is mainly determined by two aspects: (1) sulfur distribution ratio between slag and steel; (2) sulfur transfer coefficient at the interface.

Sulfur distribution ratio

At the slag-steel interface, the ratio of mass fraction of element i in steel and mass fraction of element i in slag of reaction equilibrium is written as:

$$(wt-\%i)^* = L_i[wt-\%i]^* \tag{30}$$

where $(wt-\%i)$ is the local mass fraction of element i in slag and $[wt-\%i]$ is the local mass fraction of element i in steel; L_i indicates the distribution ratio between $(wt-\%i)$ and $[wt-\%i]$. The symbol $*$ means the value is at the equilibrium status. The theoretical value of L_S can be calculated as follows [14,15,27,28]:

$$\begin{aligned}\log L_S &= \log\frac{(\%-i)^*}{[\%-i]^*} \\ &= -\frac{935}{T} + 1.375 + \log C_S + \log f_S - \log a_O\end{aligned} \tag{31}$$

where T is the temperature at the slag-steel interface; C_S stands for the sulfide capacity; a_O and f_S are the oxygen activity and the sulfur activity coefficient in steel, respectively. In this study, the Young's model [8] is applied to determine the sulfide capacity of slag C_S as shown below:

if $\Lambda < 0.8$

$$\begin{aligned}\log C_S = &-13.913 + 42.84\Lambda - 23.82\Lambda^2 - \frac{11710}{T} \\ &- 0.02223(\%-SiO_2)\end{aligned} \tag{32}$$

if $\Lambda \geq 0.8$

$$\begin{aligned}C_S = &-0.6261 + 0.4804\Lambda + 0.7197\Lambda^2 + \frac{1697}{T} \\ &- \frac{2587\Lambda}{T} + 0.0005144(\%-FeO)\end{aligned} \tag{33}$$

where Λ is the optical basicity and defined as follows [29–31]:

$$\Lambda = \frac{\sum x_1 n_1 \Lambda_1 + x_2 n_2 \Lambda_2 + \ldots}{\sum x_1 n_1 + x_2 n_2 + \ldots} \tag{34}$$

where Λ_{th} is the optical basicity of individual oxide in slag and the value is summarised in Table 1; x_{th} indicates the mole fraction of individual oxide and n_{th} is the number of oxygen atoms associated with acidic and basic oxides.

The activity coefficient f_i in steel can be obtained by the following expression [2,5]:

$$\log f_i = \sum_j e_i^j[\%-i] \tag{35}$$

where i and j represent the dissolved element in steel, including S, Al, Mn, Si, C and O. e_i^j stands for the interaction parameters between element i and j [32], and the values are listed in Table 2.

The element activity a_i in steel can be written as follows:

$$a_i = f_i[\%-i] \tag{36}$$

where i stands for the dissolved element Al, Mn, Si, C in steel. There are several methods to estimate the oxygen activity a_O. For simplification, in this present work, it is assumed that the oxygen activity is influenced by the reaction between dissolved oxygen and aluminum in steel and alumina in slag [18]:

$$2[Al] + 3[O] = (Al_2O_3) \tag{37}$$

The equilibrium constant for Eq. (37) is described as following:

$$K = exp\left(\frac{-\triangle G^0}{RT}\right) = \frac{a_{Al_2O_3}}{a_{Al}^2 a_O^3} \tag{38}$$

where $\triangle G^0$ is the change of Gibbs free energy for the reaction and the value can be determined by the expression below:

$$\triangle G^0 = -1202050 + 386.3T \tag{39}$$

The value of $a_{Al_2O_3}$ is calculated using the following equation [18]:

$$\begin{aligned}log a_{Al_2O_3} = &\frac{\{-0.275(\%-CaO) + 0.167(\%-MgO)\}}{(\%-SiO_2)} \\ &+ 0.033(\%-Al_2O_3) - 1.560\end{aligned} \tag{40}$$

Therefore, the oxygen activity can be solved by combining Eqs. (36–40).

Table 1. Optical basicity of individual oxide.

Oxide	Al_2O_3	CaO	FeO	MgO	MnO	SiO_2
Λ_{th}	0.61	1.0	0.51	0.78	0.59	0.48

Table 2. Interaction parameters.

	C	Si	Al	Mn	O	S
C	0.124	0.08	0.043	−0.012	−0.34	0.046
Si	0.18	0.11	0.058	0	−0.23	0.056
Al	0.091	0.0056	0.045	0	−6.6	0.03
Mn	−0.07	0	0	0	−0.083	−0.048
O	−0.45	0.131	−3.9	−0.021	0	−0.131
S	0.11	0.063	0.035	−0.026	−0.27	−0.028

Sulfur transfer coefficient

At the slag-steel interface, the chemical reaction rates are controlled by mass transport processes in slag and steel phases [2]. Therefore, it is necessary to obtain the sulfur mass transfer coefficients in slag and steel. Based on the Kolmogorov theory of isotropic turbulence, Lou [2] calculates the mass transfer coefficient of species i in steel and slag through the following equations:

$$k_{m,i} = cD_{m,i}^{0.5}\left(\frac{\varepsilon_l}{\nu}\right)^{0.25} \tag{41}$$

$$k_{s,i} = cD_{s,i}^{0.5}\left(\frac{\varepsilon_l}{\nu}\right)^{0.25} \tag{42}$$

where c is a constant and is 0.4 for this study [33]; $D_{m,i}$ and $D_{s,i}$ stand for the diffusion coefficient of species i in steel and slag, which are assumed to be constants as 7.0×10^{-9} m^2/s and 7.0×10^{-11} m^2/s [2,21]; ε_l is the local turbulent energy dissipation rate; ν_l is the kinematic viscosity of steel phase. Therefore, the sulfur transfer coefficient is affected by the local turbulence flow at the slag-steel interface.

Geometry and boundary condition

In this study, the effects of stirring conditions on desulfurisation efficiency are investigated in a 155-ton gas-stirred ladle based on a Nucor Decatur ladle. The ladle used in this study is shown in Figure 1. The diameter of the bottom surface D is 3.25 m. There are two plugs at the bottom surface. In this study, two different plug separation angles are investigated: 90 ° and 180 ° as shown in Figure 2. The distance between the plug and the centre of the bottom surface

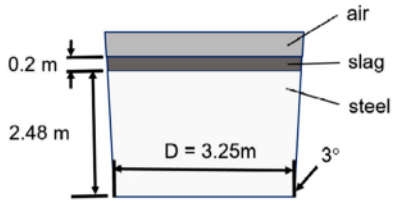

Figure 1. Schematic diagram of Nucor simplified generic ladle.

is 0.28 times the diameter of the bottom surface. The diameter of each plug is 0.0754 m.

There are two types of boundary conditions: the top surface is treated as a pressure-outlet with gas phase backflow. The other boundaries are set to be the no-slip wall. The backflow turbulent intensity is set to be 5%, and the backflow turbulent viscosity ratio is set to be 10. For the discrete bubble particle, the surface injection release method is used at the plug area. The top surface is considered to be the escape type to make argon leave the domain. The type of other boundaries is reflect for the discrete phase, as shown in Figure 3. There is finer mesh at the slag-steel interface, the slag-air interface, and the inlet surface and bubble-liquid plume zone.

The other parameters employed in this study are listed in Table 3 provided by Nucor company. Two different argon gas flow rates are used in this study: 5 SCFM (2.23×10^{-3} Nm3/s) and 20 SCFM (8.92×10^{-3} Nm3/s). By combing the plug separation angle and argon flow rate of each plug, there are totally 6 cases investigated in terms of desulfurisation process as listed in Table 4. It is assumed that the temperature at the slag-steel interface is homogenised and keeps constant during the ladle refining process and the influence of temperature gradient is not taken into account [2,4,21]. The initial compositions of steel and slag are summarised in Table 5 based on Lou and Zhu's study [2].

Numerical procedure

The commercial CFD software ANSYS Fluent 2020R1 is used to simulate the multiphase flow and interface behaviours, and the user-defined function (UDF) is utilised to calculate the sulfur source terms by desulfurisation process at the slag-steel interface. The transient pressure-based solver is applied to simulate the multiphase flow in a gas-stirred ladle with slag, steel and gas phases. The interface modelling type is sharp and the volume fraction formulation is explicit with the discretisation method of geo-reconstruct spatial [21]. The PRESTO! method is used for solving the pressure equation. The fixed time step is used and the size is set to be 0.0001 s. During iteration, the convergence is assumed to reach a point where all the absolute scaled residuals are

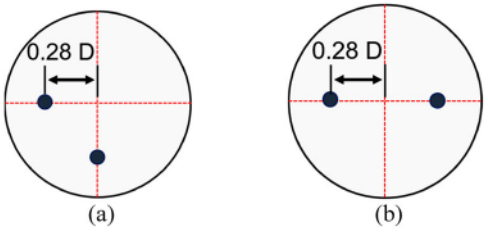

Figure 2. Schematic diagram of different plug separation angles. (a) 90°; (b) 180°.

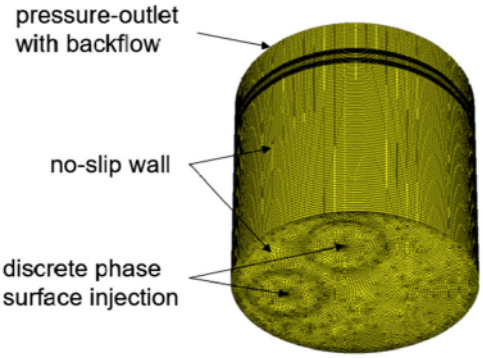

Figure 3. Schematic diagram of mesh and boundary condition.

Table 3. Parameters employed in the CFD simulation.

Density of steel	6975 kg/m^3
Density of slag	2786 kg/m^3
Density of argon	0.719 kg/m^3
Viscosity of steel	0.006 kg/(m-s)
Viscosity of slag	0.06 kg/(m-s)
Viscosity of argon	2.125×10^{-5} kg/(m-s)
Surface tension coefficient between steel and slag	1.15 N/m
Surface tension coefficient between steel and argon	1.823 N/m
Temperature	1833K

Table 4. Ladle stirring condition.

	Plug separation angle (°)	Argon flow rate
Case 1	90	5–5 SCFM
Case 2	180	5–5 SCFM
Case 3	90	5–20 SCFM
Case 4	180	5–20 SCFM
Case 5	90	20–20 SCFM
Case 6	180	20–20 SCFM

Table 5. Initial chemical composition of steel and slag.

Species	Steel composition (%)
S	0.0107
Al	0.058
Mn	0.66
Si	0.18
C	0.35
Species	Slag composition (%)
Al_2O_3	21.32
MnO	0.24
SiO2	5.84
CaO	57.79
MgO	6.02
FeO	0.95
S	0.07

smaller than 10^{-3}. Besides, the sulfur mass is checked by combining the removed sulfur mass obtained from Eq. (28) and the sulfur mass remained in steel from Fluent: if the difference between the initial sulfur mass and the sum of these two values is less than 0.5%, the simulation result is acceptable.

The mesh sensitivity has been carried out using meshes with different cell numbers: 323,000, 625,000 and 809,000. Figure 4 shows the velocity magnitude in Case 6 at the height of 1.5 m. The difference of the results with the mesh of 809,000 and 625,000 are smaller than 1.25%. However, the maximum difference of velocity obtained by 323,000 cells and 809,000 cells is higher than 7.29%. The average turbulent dissipation rates at the interface with different meshes are also summarised in Table 6. It can be seen from Table 6 that the difference of average ε is higher than 10%

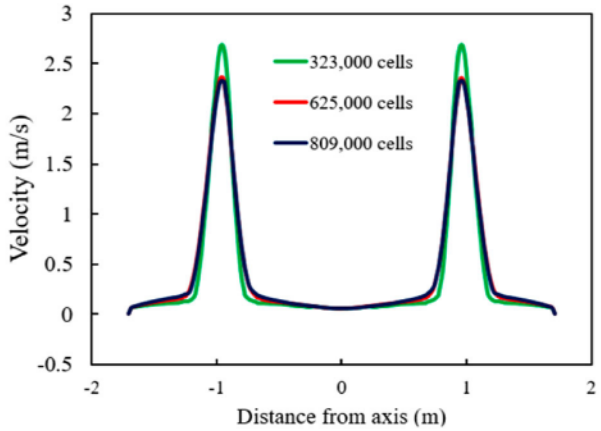

Figure 4. Velocity magnitude at the height of 1.5 m in Case 6 with different meshes

between 323,000 cells and 809,000 cells; while when using 625,000 cells and 809,000 cells, the difference is less than 1.2%. Therefore, the mesh with 625,000 cells is used for investigating the desulfurisation efficiency with different stirring conditions.

To save computational time and resources, a simplification used in Lou and Zhu's work [2] is applied to this model: the specie distribution is considered to be homogeneous because of the small size of slag layer compared to the liquid steel, and the species content is calculated by UDF through the following equation:

$$(\%-S)=\frac{W_{S,0}(\%-S)_0-W_m\left(\int_{V_{cell}}[\%-S]dV_{cell}-\int_{V_{cell}}[\%-S]_0dV_{cell}\right)}{W_S} \quad (43)$$

where $(\%-S)_0$is the initial mass fraction of sulfur in slag phase; $[\%-S]_0$ is the initial mass fraction of sulfur in steel phase; W_m is the weight of steel phase; W_S is the weight of slag phase and can be calculated by the following equation:

$$W_S=W_{S,0}-\sum_i W_m\left(\int_{V_{cell}}\frac{[\%-S]}{100}dV_{cell}-\int_{V_{cell}}\frac{[[\%-S]_0}{100}dV_{cell}\right) \quad (44)$$

More details can be found in the reference [2]. After becoming a quasi-steady state, the flow characters, including velocity, turbulence and interface shape, are not calculated anymore to save computational time, and the desulfurisation rate as well as slag compositions is solved by the UDF [2] until reaching the final refining moment.

To determine the quasi-steady state, the average velocities of 3 layers with different heights, 0.8, 1.6 and 2.4 m, are monitored. Figure 5 shows the velocities on different layers with time in the 180° 20–20 SCFM case. It can be noticed that the velocity magnitudes almost remain constants after 32 s, and therefore it is at the quasi-steady state.

Table 6. Average turbulent dissipation rate at the slag-steel interface in different cases.

Cell number	Average ε at Interface (m^2/s^3)
323,000	2.217×10^{-1}
625,000	2.028×10^{-1}
809,000	2.004×10^{-1}

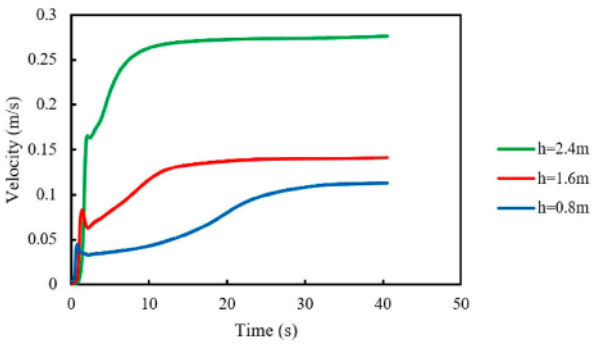

Figure 5. Velocity magnitudes on layers with different heights in the 180° 20–20 SCFM case with time

Simulation results and discussion

Validation

The industrial measurement shows that the slag eye diameter is 0.73 m in a Nucor generic ladle with 180° plug separation angle and 30 SCFM argon flow rate. The simulation result of the current model shows the predicted slag eye diameter is 0.79 m, with a percentage error of 7.5%, showing great agreement with the plant trial. Because the slag eye is formed by the plume momentum transfer, the slag eye size can reflect the interface behaviours. The desulfurisation only occurs at the slag-steel interface, the flow field at the interface is important. Hence, this multiphase model can predict the multiphase flow at the interface for desulfurisation investigation.

The accuracy of the desulfurisation prediction is investigated by comparing the simulation results of this current model with the predicted values from Lou's model and measured data [2]. The desulfurisation process in two scenarios, Run-1 and Run-4, with different chemical compositions in slag and steel [2], are simulated by this model and the results are shown in Figure 6. It indicates that the simulation results by the current model agree well with both Lou's results and measured data, showing good behaviour of this model for predicting the desulfurisation process in a gas-stirred ladle.

After validation, the current model can be applied to explore the impacts of different stirring conditions on desulfurisation process in a gas-stirred ladle as shown in Figure 1.

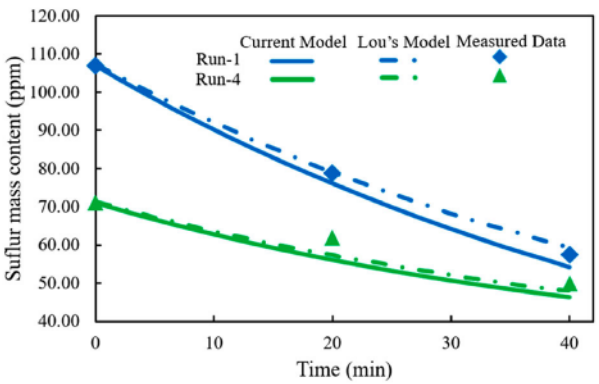

Figure 6. Comparison of sulfur mass content predicted by current model and Lou's model [2] with measured data.

The initial compositions of steel and slag are listed in Table 5. As mentioned above, 6 cases are investigated and the stirring conditions are summarised in Table 3. The desulfurisation treatment in this study is 40 min as in Lou and Zhu's study [2].

Kinetic behaviour of different stirring conditions

In this model, it is assumed that when the volume fraction is higher than 0.5, the cell is considered to be filled with steel phase, and therefore the steel domain and slag-steel interface can be found. Figure 7 shows the steel velocity in different cases. Under the impact of argon stirring, steel velocity is high at the plug zones and gradually decreases along each argon-bubble plume from the bottom to the interface. However, at the bump region of the interface, the steel velocity is shallow, indicating that the slag layer is impeding vertical flow and that the kinetic energy is being used to promote slag layer deformation and the development of slag eyes.

To better explore the impacts of plug separation angle and argon flow rate on steel velocity with different plug separation angles, the velocities along a line across two plugs at a certain height are monitored. The monitoring lines are shown in Figure 8.

The velocity magnitudes of different cases at the heights of 0.8 and 1.6 m are shown in Figure 9. It can be found that when the argon flow rate combination is 5–5 SCFM, the velocity magnitudes in the bubble plume are almost the same between 90° and 180°, as shown in Figure 9(a) and (b). When using the 5–20 SCFM argon flow rate, the peak values of velocity in the plume zone with 180° plug separation angle are slightly higher than those with 90° plug separation angle at h = 0.8 m, as indicated in Figure 9(c). At h = 1.6 m, the highest velocity in the 5 SCFM argon plume zone with 180° plug separation angle is also slightly bigger than that with 90° plug separation angle, as shown in Figure 10 (d). Larger velocity magnitudes are observed in the 180° 20–20 SCFM case than the 90° 20–20 SCFM case, as shown in Figure 9(e) and (f). Therefore, the maximum velocity with 180° plug separation angle is higher than that with 90° plug separation angle under the same argon flow rate. This phenomenon is because since the two plumes in the 90° angle ladle are closer to each other than those in the 180° angle ladle, the rising steel stream is more susceptible to

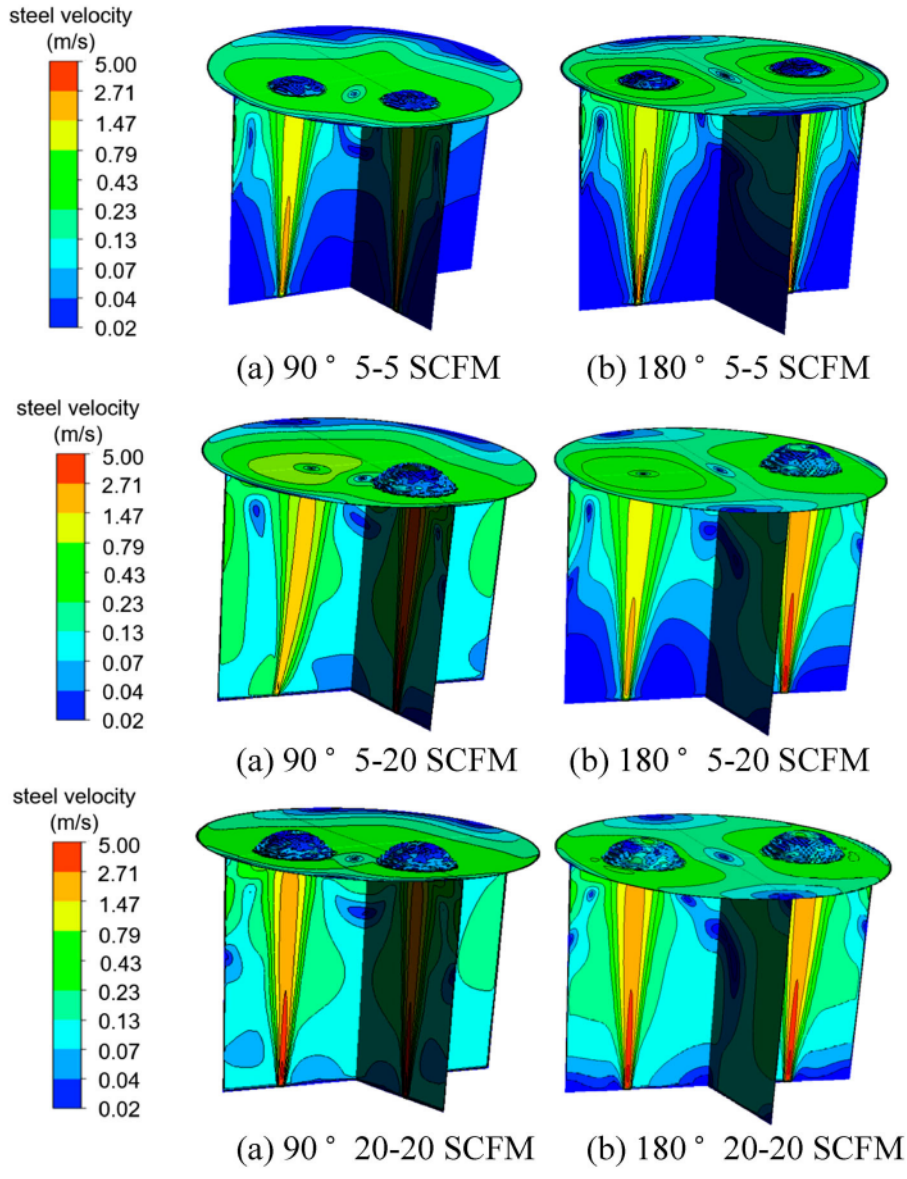

Figure 7. Steel velocity of different scenarios in quasi-steady state. (a) Case 1. 90° 5–5 SCFM; (b) Case 2. 180° 5–5 SCFM; (c) Case 3. 90° 5–20 SCFM; (d) Case 4. 180° 5–20 SCFM; (e) Case 5. 90° 20–20 SCFM; (f) Case 6. 180° 20–20 SCFM

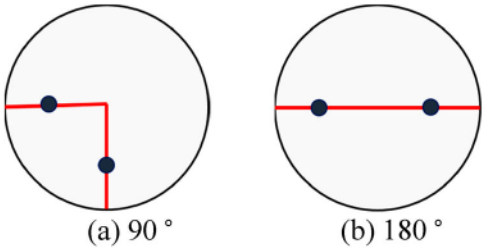

Figure 8. Monitor lines across two plugs with different plug separation angles. (a) 90°; (b) 180°

the backflow generated by the other stream, so the velocity peak is slightly smaller.

Figure 10 depicts the mass transfer coefficient in steel phase $k_{m,S}$ at the interface: from the centre of the plume to the sidewall, $k_{m,S}$ slightly rises and then keeps decreasing. Because the $k_{m,S}$ is proportional to the steel turbulent dissipation rate as specified in Eq. (41), the local $k_{m,S}$ distribution at the interface can reflect the turbulent dissipation distribution as well.

Table 7 displays the average $k_{m,S}$ values at the slag-steel interface for various cases. It can be noticed that the average $k_{m,S}$ slightly rises when the plug separation angle is adjusted from 90° to 180° by comparing the value in Case 1 and Case 2, indicating that species are transported more effectively from the zone near the interface to the interface. Similar conclusions are found according to the comparison between Case 3 and Case 4 and the comparison between Case 5 and Case 6. This phenomenon can be explained by the fact that when the separation angle is 180°, the distance between two plumes is bigger than that with 90°, and the interactions between two plumes are smaller. Therefore, the plume is widely dispersed with 180° plug angle, and the $k_{m,S}$ is more uniform at the slag-steel interface, as shown in Figure 10, and thereby the average $k_{m,S}$ is bigger. Therefore, in all cases investigated in this section, 180° plug separation angle is better than 90° plug separation angle terms of interfacial species transport process. In addition, when the plug separation angle is 90°, a bigger average $k_{m,S}$ is formed by a higher argon flow rate referring to Case 1, Case 3 and Case 5: when the argon flow rate rises from 5/5 SCFM to 5/20 SCFM, the $k_{m,S}$ value rises by 24.86%, and when the argon flow rate increases from 5/5 SCFM to 20/20 SCFM, the $k_{m,S}$ value rises by 47.06%. Consistent findings are yielded based on the $k_{m,S}$ values in Case 2, Case 4 and Case 6.

Based on Eq. (29), $k_{eff,S}$ is affected by L_S, $k_{m,S}$ and $k_{s,S}$. With the same initial compositions listed in Table 5, the values of L_S are the same in different cases based on Eqs. (31)–(40). According to Eqs. (41) and (42), $k_{s,S}$ is proportional to $k_{m,S}$ and $k_{s,S} = 0.1 k_{m,S}$ [2,21]. Thus, a higher $k_{m,S}$ leads to a higher $k_{eff,S}$.

Desulfurisation behaviour of different stirring conditions

Figures 11 and 12 show the change of sulfur mass content with time in liquid steel and the sulfur removal ratio at t = 40 min calculated by Eq. (45) [2] in the 155-ton gas-stirred ladle under different stirring conditions, respectively. It can be found by comparing Case 1 and Case 2 that when the argon flow rate is 5–5 SCFM, the final sulfur content is 68.80 ppm with 180 ° plug separation angle and 71.86 ppm with 90 ° plug separation angle. The sulfur removal ratio

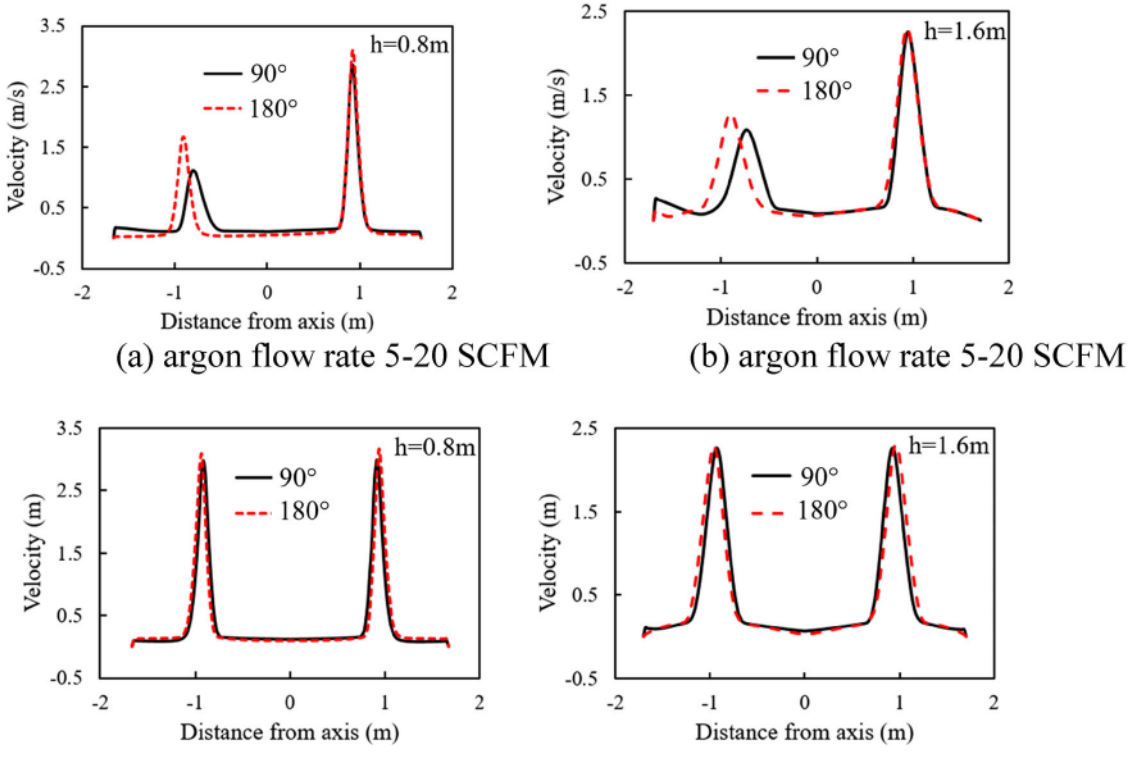

Figure 9. Velocity along the monitor line at different height. (a) 90° 5–5 SCFM & 180° 5–5 SCFM, h = 0.8 m; (b) 90° 5–5 SCFM & 180° 5–5 SCFM, h = 1.6 m; (c) 90° 5–20 SCFM & 180° 5–20 SCFM, h = 0.8 m; (d) 90° 5–20 SCFM & 180° 5–20 SCFM, h = 1.6 m; (e) 90° 20–20 SCFM & 180° 20–20 SCFM, h = 0.8 m; (f) 90° 20–20 SCFM & 180° 20–20 SCFM,, h = 1.6m

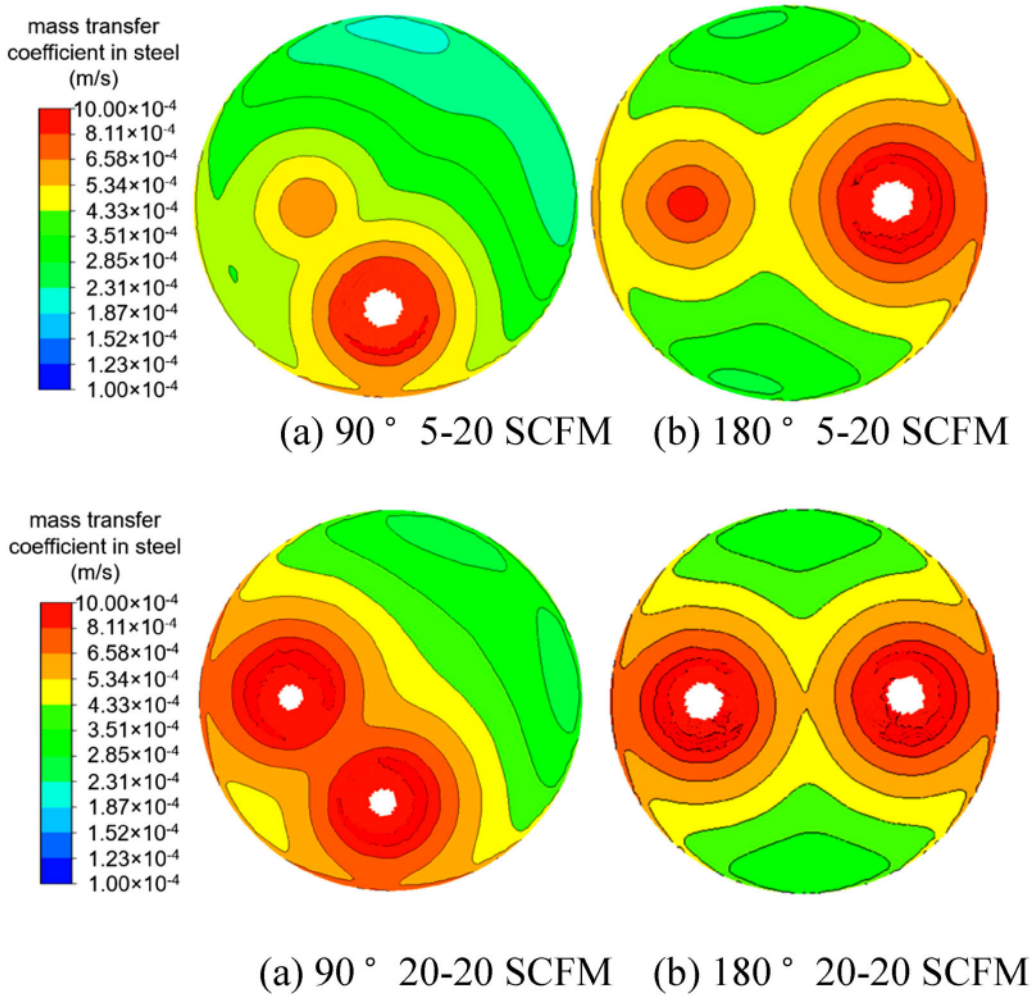

Figure 10. Mass transfer coefficient of species in steel phase of different scenarios in quasi-steady state. (a) Case 1. 90° 5–5 SCFM; (b) Case 2. 180° 5–5 SCFM; (c) Case 3. 90° 5–20 SCFM; (d) Case 4. 180° 5–20 SCFM; (e) Case 5. 90° 20–20 SCFM; (f) Case 6. 180° 20–20 SCFM.

increases from 32.84% to 35.70% when changing the plug separation angle from 90° to 180°. Therefore, the 180° plug separation angle has better desulfurisation behaviour than the 90° plug separation angle. Similarly, the comparison between Case 3 and Case 4 and the comparison between Case 5 and Case 6 show that the 180° plug separation angle always results in lower sulfur content and higher sulfur removal ratio than the 90° plug separation angle when the gas flow rate is 5–20 SCFM or 20–20 SCFM. Therefore, in all the cases discussed in this study, a more effective desulfurisation process is obtained by using the 180° plug separation angle rather than the 90° plug separation angle.

Furthermore, it can be seen by comparing Case 1 and Case 3 that when the separation angle is 90°, the final sulfur content decreases from 71.86 to 65.62 ppm with the growth of the argon flow rate from 5–5 SCFM to 5–20 SCFM, and the sulfur removal ratio rises from 32.84% to 38.20%; when the argon flow rate increases to 20–20 SCFM, as shown in Case 5, the final sulfur content reaches 60.72 ppm, and the sulfur removal ratio grows to 43.25%. Therefore, in the scenarios investigated in this paper, when the separation angle is 90°, the final sulfur content can be reduced by increasing the argon flow rate. Similarly, it can be noticed from the simulation results of Case 2, Case 4 and Case 6, when the separation angle is 180°, a higher argon flow rate produces a lower sulfur content and a bigger sulfur removal ratio.

Table 7. Average $k_{m,S}$ on slag-steel interface in different cases.

Scenario	Average $k_{m,S}$ (m/s)
Case 1: 90° 5–5 SCFM	4.131×10^{-4}
Case 2: 180° 5–5 SCFM	4.216×10^{-4}
Case 3:90° 5–20 SCFM	5.158×10^{-4}
Case 4: 180° 5–20 SCFM	5.533×10^{-4}
Case 5:90° 20–20 SCFM	6.075×10^{-4}
Case 6: 180° 20–20 SCFM	6.351×10^{-4}

$$\varphi = \frac{[\%-S]_0 - [\%-S]_t}{[\%-S]_0} \times 100\% \tag{45}$$

Furthermore, it can be seen by comparing Case 1 and Case 3 that when the separation angle is 90°, the final sulfur content decreases from 71.86 ppm to 65.62 ppm with the growth of the argon flow rate from 5–5 SCFM to 5–20 SCFM, and the sulfur removal ratio rises from 32.84% to 38.20%; when the argon flow rate increases to 20–20 SCFM, as shown in Case 5, the final sulfur content reaches 60.72 ppm, and the sulfur removal ratio grows to 43.25%. Therefore, in the scenarios investigated in this paper, when the separation angle is 90°, the final sulfur content can be reduced by increasing the argon flow rate. Similarly, it can be noticed from the simulation results of Case 2, Case 4 and Case 6, when the separation angle is 180°, a higher argon flow rate produces a lower sulfur content and a bigger sulfur removal ratio.

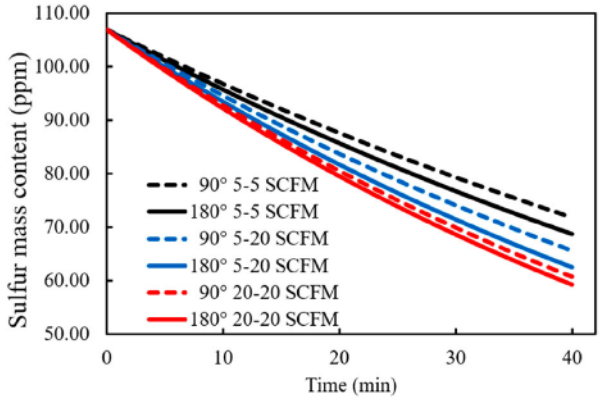

Figure 11. Predicted sulfur mass content with time in 155 ton ladle for different stirring conditions.

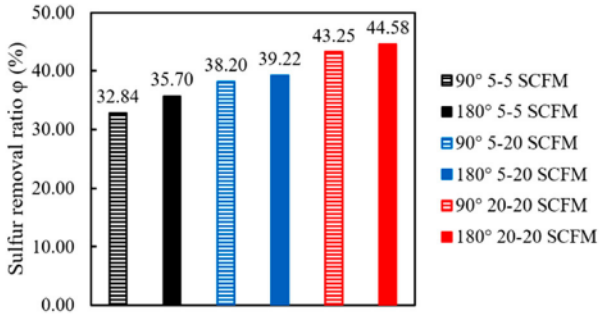

Figure 12. Predicted sulfur removal ratio in 155 ton ladle for different stirring conditions, t = 40 min.

Based on the desulfurisation behaviours discussed above, it can be concluded that a higher argon flow rate is beneficial to the improvement of sulfur removal efficiency and the 180° plug separation angle is better than the 90° plug separation angle in terms of desulfurisation rate. These are because: the value of $k_{m,S}$ can be significantly increased by increasing the argon flow rate, as can be seen from Figure 10 and Table 7; according to Eqs. (41) and (42), with the same local turbulence dissipation rate and kinematic viscosity, $k_{s,S} = 0.1k_{m,S}$, and thereby $k_{s,S}$ also increases with the growth of $k_{m,S}$, which means a higher turbulence dissipation rate leads to higher $k_{m,S}$ and $k_{s,S}$, promoting the species transfer rates in steel phase and slag phase. Based on Eq. (29), a bigger $k_{m,S}$ also results in a higher $k_{eff,S}$, indicating that a larger turbulence dissipation rate also improves the species transfer coefficient between slag and steel phases, and consequently enhances the sulfur removal efficiency. When the plug separation angle is adjusted from 90° to 180°, the distribution of $k_{m,S}$ on the slag-steel interface is more evenly distributed, and consequently increasing the the average interfacial $k_{m,S}$, as shown in Figure 10 and Table 7, thus also making $k_{eff,S}$ become bigger and helping to improve the desulfurisation rate. In addition, according to the results in Figure 9, the velocity of steel with the 180° plug separation angle is slightly higher than that with the 90° plug separation angle under the same gas flow rate, which also facilitates the sulfur transfer process to the slag-steel interface, promoting the desulfurisation rate as well.

Conclusion

The desulfurisation processes during secondary steelmaking in a ladle metallurgical furnace have been investigated using a 3D multiphase computational fluid dynamics model by considering the influence of distorts in the slag-steel surface on interfacial species transport. The model can predict the multiphase flow field and the shape of the interface at a quasi-steady state and estimate the reaction region, and then the desulfurisation rate is calculated. The model is validated by plant data and simulation results from literature work. The impacts of different stirring conditions on the desulfurisation rate are explored in a Nucor simplified ladle by this model. The results show that when the argon flow rate is the same, the 180° plug separation angle leads to a higher desulfurisation efficiency than the 90° plug separation angle; when the plug separation angle keeps unchanged, the desulfurisation rate can be improved by increasing the argon flow rate from 5–5 SCFM to 5–20 SCFM to 20–20 SCFM.

Acknowledgements

The authors would like to thank NSF-GOALI grant (CMMI-2113967), the Steel Manufacturing Simulation and Visualization Consortium (SMSVC), the SMSVC Ladle Project Technical Committee members, and Nucor Steel for supporting this research and for permission to publish this work.

Disclosure statement

No potential conflict of interest was reported by the author(s).

Funding

This work was supported by National Science Foundation: [Grant Number CMMI-2113967]; Steel Manufacturing Simulation and Visualization Consortium (SMSVC).

References

[1] Roy D, Pistorius P, Fruehan R. Effect of silicon on the desulfurization of Al-killed steels: part I. mathematical model. Metall Mater Trans B. 2013;44:1086–1094.
[2] Lou W, Zhu M. Numerical simulation of desulfurization behavior in gas-stirred systems based on computation fluid dynamics–simultaneous reaction model (CFD–SRM) coupled model. Metall Mater Trans B. 2014;45:1706–1722.
[3] Cao Q, Nastac L. Mathematical investigation of fluid flow, mass transfer, and slag-steel interfacial behavior in gas-stirred ladles. Metall Mater Trans B. 2018;49:1388–1404.
[4] Wang Q, He Z, Li G, et al. Numerical investigation of desulfurization behavior in electroslag remelting process. Int J Heat Mass Transfer. 2017;104:943–951.
[5] Conejo A, Lara F, Macias-Hernández M, et al. Kinetic model of steel refining in a ladle furnace. Steel Res Int. 2007;78:141–150.
[6] Fincham C, Richardson F. The behaviour of sulphur in silicate and aluminate melts. Proceed R Soc Lond A Math Phys Sci. 1954;223:40–62.
[7] Sosinsky D., Sommerville I. The composition and temperature dependence of the sulfide capacity of metallurgical slags. Metall Trans B. 1986;17:331–337.
[8] Young R, Duffy J, Hassall G, et al. Use of optical basicity concept for determining phosphorus and sulphur slag-metal partitions. Ironmak Steelmak. 1992;19:201–219.
[9] N MM, S DU, Seetharaman S. Sulphide capacities of "FeO"-SiO_2, CaO-"FeO", and "FeO"-MnO slags. ISIJ Int. 1999;39:657–663.
[10] Taniguchi Y, Sano N, Seetharaman S. Sulphide capacities of CaO–Al_2O_3–SiO_2–MgO–MnO slags in the temperature range 1673–1773K. ISIJ Int. 2009;49:156–163.
[11] Park J. Structure–property correlations of CaO–SiO_2–MnO slag derived from Raman spectroscopy. ISIJ Int. 2012;52:1627–1636.
[12] Shi C, Yang X, Jiao J, et al. A sulphide capacity prediction model of CaO–SiO_2–MgO–Al_2O_3 ironmaking slags based on the ion and molecule coexistence theory. ISIJ Int. 2010;50:1362–1372.

[13] Inoue R, Suito H. Sulfur partitions between carbon-saturated iron melt and Na_2O-SiO_2 slags. Trans Iron Steel Inst Japan. 1982;22:514–523.
[14] Chan A, Fruehan R. The sulfur partition ratio and the sulfide capacity of Na_2O-SiO_2 slags at 1200 C. Metall Trans B. 1986;17:491–496.
[15] Andersson M, Jönsson P, Nzotta M. Application of the sulphide capacity concept on high-basicity ladle slags used in bearing-steel production. ISIJ Int. 1999;39:1140–1149.
[16] Jeong T, Cho J, Heo J, et al. Desulfurization behavior of Si-killed 316L stainless steel melt by CaO-SiO_2-CaF_2-Al_2O_3-MgO slag. J Mater Res Technol. 2022;18:2250–2260.
[17] Jonsson L, Sichen D, Jönsson P. A new approach to model sulphur refining in a gas-stirred ladle–a coupled CFD and thermodynamic model. ISIJ Int. 1998;38:260–267.
[18] Andersson M, Jonsson L, Jönsson P. A thermodynamic and kinetic model of reoxidation and desulphurisation in the ladle furnace. ISIJ Int. 2000;40:1080–1088.
[19] Andersson M, Hallberg M, Jonsson L, et al. Slag-metal reactions during ladle treatment with focus on desulphurisation. Ironmak Steelmak. 2002;29:224–232.
[20] Singh U, Anapagaddi R, Mangal S, et al. Multiphase modeling of bottom-stirred ladle for prediction of slag–steel interface and estimation of desulfurization behavior. Metall Mater Trans B. 2016;47:1804–1816.
[21] Cao Q. Mathematical modeling of the fluid flow, multicomponent slag-metal reactions and desulfurization efficiency in gas-stirred ladles [PhD thesis]. Tuscaloosa (AL): The University of Alabama; 2018.
[22] Cao Q, Nastac L, Pitts-Baggett A, et al. Numerical investigation of desulfurization kinetics in gas-stirred ladles by a quick modeling analysis approach. Metall Mater Trans B. 2018;49:988–1002.
[23] Oliveira Pezzin R, Berger A, Grillo F, et al. Analysis of the influence of the solid and liquid phases on steel desulfurization with slags from the CaO–Al_2O_3 systems using computational thermodynamics. J Mater Res Technol. 2020;9:838–846.
[24] Moosavi-Khoonsari E, Van Ende M, Jung I. Kinetic simulation of hot metal pretreatment: desulfurization using powder injection. Metall Mater Trans B. 2022;53:981–998.
[25] Jia S, He Z, Ouyang D, et al. Powder injection effect on Hot metal desulfurization behavior in the Kanbara reactor: a transient 3D coupled numerical model. ISIJ Int. 2022;62:449–456.
[26] Cao Q, Nastac L. Mathematical modeling of the multiphase flow and mixing phenomena in a gas-stirred ladle: the effect of bubble expansion. JOM. 2018;70:2071–2081.
[27] Andersson M, Jönsson P, Hallberg M. Optimisation of ladle slag composition by application of sulphide capacity model. Ironmak Steelmak. 2000;27(27):286–293.
[28] Vuolio T, Visuri V, Paananen T, et al. Identification of rate, extent, and mechanisms of Hot metal resulfurization with CaO-SiO 2-Na 2 O slag systems. Metall Mater Trans B. 2019;50:1791–1807.
[29] Ghosh D, Krishnamurthy V, Sankaranarayanan S. Application of optical basicity to viscosity of high alumina blast furnace slags. J Min Metall Sect B. 2010;46:41–49.
[30] Mori T. On the phosphorus distribution between slag and steel. Bull Jap Inst Metals. 1984;23:354–361.
[31] Krishna Y, Sowmya T, Sankaranarayanan S. Application of optical basicity parameter to foaming of slags. Metall Ital. 2008;10:51–54.
[32] Engh T. Principles of metal refining. Oxford: Oxford University Press; 1992. p. 62–63.
[33] Lamont J, Scott D. An eddy cell model of mass transfer into the surface of a turbulent liquid. AIChE J. 1970;16:513–519.